

25th International Meshing Roundtable (IMR25)

Block topology generation for structured multi-block meshing with hierarchical geometry handling

Zaib Ali^{a,*}, James Tyacke^a, Paul G. Tucker^a, Shahrokh Shahpar^b^a*Department of Engineering, University of Cambridge, Cambridge, CB2 1PX, United Kingdom.*^b*CFD Methods, DSE, Rolls-Royce, plc., Derby, England DE24 8BJ, United Kingdom.*

Abstract

Multi-block structured mesh generation remains one of the most popular meshing techniques because of its superior simulation quality but it is difficult to apply when dealing with complex three dimensional (3D) domains. To this end, a hybrid blocking approach, combining the medial axis based method with level set isosurface is presented and applied to mesh complex 3D external flow domains. Secondly, a hierarchical geometry handling approach is demonstrated which makes use of the lower order modeling, overset meshes and zonal blocking to reduce the meshing and modeling effort. Typical external aerodynamics cases have been showcased to describe how such techniques can be used for efficiently addressing modern industrial meshing challenges.

© 2016 The Authors. Published by Elsevier Ltd.

Peer-review under responsibility of organizing committee of the 25th International Meshing Roundtable (IMR25).

Keywords: Multi-Block Structured Meshing, Medial Axis Transform, Automatic Blocking, Wall Distance.

1. Introduction

Mesh generation has remained one of the most time consuming steps for flow simulations and faces even bigger challenges with the ever increasing need for simulating complex 3D flows. There is a trade-off between the mesh quality, ease of generation, solver requirements and parallel mesh generation when choosing amongst the structured and unstructured mesh types. Unstructured meshes offer more flexibility for meshing complex 3D domains. Structured meshes, on the other hand, offer higher numerical accuracy and less storage than the unstructured meshes. They also allow relatively easy implementation of high-order finite volume and finite difference schemes.

Multi-block structured mesh generation is among the most widely used meshing techniques in flow simulations. This is essentially a two-stage process. In the first stage, a suitable blocking topology is generated which divides the complex domain into simple sub-domains. The resulting blocks are subsequently meshed. This structured blocking offers an efficient meshing strategy for topologically simple configurations and standard templates exist for partitioning of such domains. For example, the H-O-H type blocking is commonly used to mesh the turbine blade passage. However, the modern day design challenges demand the computational analysis of more realistic geometries. Aero-engine domains, for example, involving the fan, outlet guide vanes, gearbox shaft and nozzle coupled with wing,

*Corresponding author.

E-mail address: zaibali@gmail.com

flap and pylon are now being used for flow simulations. Meshing such multiply linked and more diverse geometries requires significant user intervention, or writing of templates as part of a library [1]. Thus, an automatic or semi-automatic blocking strategy can be beneficial to reduce the CFD design cycle time and could be a better alternative to the unstructured or hybrid meshing methods.

Fully automatic 3D block topology generation is a complex problem and currently there is no ideal block topology algorithm with all the desired features for structured mesh generation. However various automatic blocking approaches have been proposed with varying levels of automation and geometric complexity handling. This includes approaches based on medial axis [2–5], paving/plastering [6,7] and more recently methods based on cross/frame field [8,9].

The medial axis transform (MAT) based algorithms for the domain decomposition have been presented in, for example, [2–5]. Here the medial axis is generated using the Voronoi based method. A subdivision is created resulting in one block for each medial vertex, medial edge and medial face. A midpoint subdivision is then used for meshing the blocks. An alternative has been presented by Rigby [10], called the ‘TopMaker’ approach, which makes use of medial vertices and parts of medial axis to block the domain. Medial vertices are defined as the points which are equidistant from three locations from the domain boundary. Consequently, six types of medial edges and appropriate rules are defined for creating the blocks. Further enhancements have been included to produce a good quality mesh however this technique has yet to be extended for 3D.

Distance field based approaches are also widely used for the medial axis approximation and domain decomposition [11–13]. A hybrid approach called differential MAT or d-MAT approach is presented in Xia and Tucker [14,15]. Here, the hyperbolic-natured eikonal, level set equation is used to calculate the distance field [16]. Medial axis point clouds are then extracted from the Laplacian or Hessian determinant of the distance field. A thinning algorithm is then used for thinning the point clouds into curves and surfaces. The method is illustrated in the Figure 1(a-c) for a simple domain. Such a hybrid approach thus avoids complexity of pure geometric approach and provides more accuracy than the pure image thinning algorithms. The differential equation based distance field and subsequent medial axis approximations have the advantage that a customized medial axis can be computed by manipulating the boundary conditions. This is shown in Figure 1(d) where the distance field relative to the part having the wall boundary condition is computed. This results in the simpler medial axis represented by the red curves in the Figure 1(f) thus avoiding triangular blocks encountered in, for example, Figure 1(c). In addition to the collision of wave fronts forming the compression shocks i.e. the medial axis, the expansion waves shown in the Figure 1(e) can be utilized to aid the blocking process. The expansion features are connected to the nearest ‘medial vertex’; that is if that point lies within sight of the fan caused by the expansion feature. If not, it is connected to the nearest point on the shock feature topology (see green lines as Rule 1 in Figure 1(f)). Rule 2 is borrowed from the TopMaker method [10]; Hanging features (features which are not connected to anything) are extended to the nearest point on the geometry. This is shown by the green line in Figure 1(g).

Recent advancements in mesh generation are the methods based on the cross-fields (frame fields in 3D). A cross field is defined by assigning a set of four unit vectors to points at the discrete locations. These unit vectors form a regular cross on the tangent plane. Thus the size and the orientation of the quadrilateral cells can be specified by the cross field. A number of approaches have been put forward for 2D and 3D cross field based domain decomposition and mesh generation. To generate the block topology, the partitioning created by connecting the cross-field streamlines to the singularities can be used. The resulting blocks of the cross field can then be mapped to a grid. Such methods have been presented in, for example, [8,17–21]. The cross field approach towards domain decomposition and mesh generation is novel and efficient but quite complex and expensive. LayTracks3D [22], is a hybrid hexahedral meshing method combining medial axis based decomposition and the advancing front method. This technique produces good quality hexahedral meshes but degenerate cells can be formed around the sharp concave features.

Malcevici [23] presents another automated blocking strategy based on a Cartesian fitting method. While preserving the topology definition, a forward geometry simplification is performed followed by fitting the model into a Cartesian framework. The next step is blocking the domain after which the blocked model is mapped back on to the original geometry. Further operations such as removing singularities by J-grid wrapping are performed to enhance the mesh quality. This technique has been applied for meshing the end-wall cavities found in turbomachinery. This technique is very simple and but has only been demonstrated for 2D cases so far. The method sometimes produces some unnecessary mesh clustering across the block interfaces.

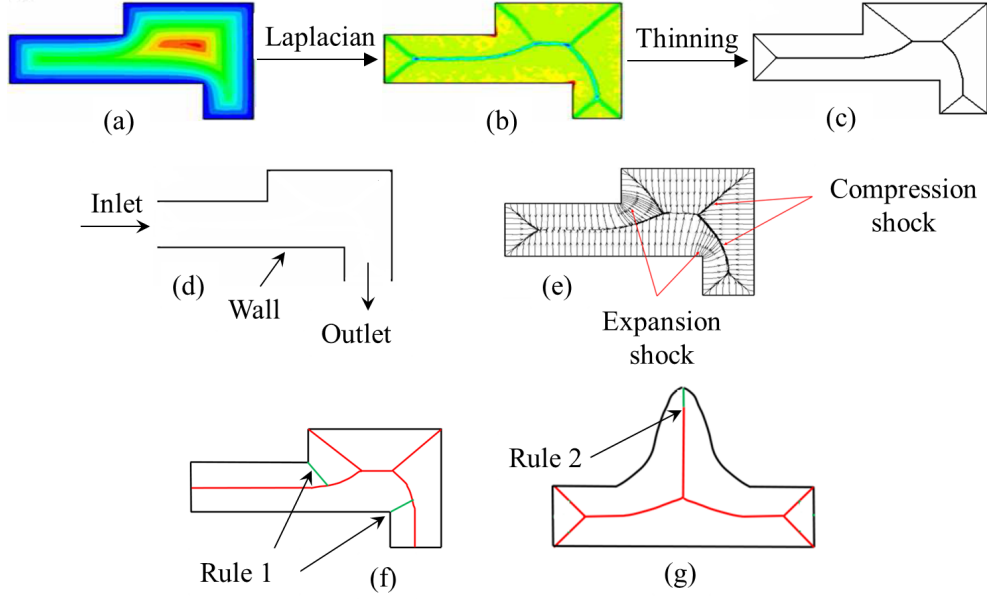


Fig. 1: d-MAT method and blocking; (a) distance field of a simple domain (b) medial axis extraction through the distance field Laplacian (c) point cloud thinning (d) simplified medial axis (e) shock and expansion features of the wave fronts (f) blocking rule 1 (g) blocking rule 2.

An assessment of various automatic block topology generation techniques surveyed above has been performed in [24,25]. The comparison has been carried out using an adjoint based error analysis of the meshes generated by these block topologies. It is found that, in general, the medial axis based approaches provide optimal blocking and yields better accuracy in computing the functional of interest. Mostly, domains having internal flows were used for this assessment. However, the medial axis based methods may not always yield an optimal block topology when dealing with complex 3D geometries and external flows. To overcome this limitation, a hybrid blocking technique is illustrated which makes use of the distance field isosurface in addition to the medial axis transform. This is demonstrated using a wing-body-tail and a jet-wing-flap configurations. In addition to that, to reduce the meshing effort, a hierarchical geometry handling approach is also defined and applied to an engine-wing-flap configuration. These approaches are described next.

2. Methodology

2.1. Novel hybrid blocking

Consider an aero-engine jet-wing-flap (JWF) domain with a far-field as shown in the Figure 2. The medial axis close to the JWF geometry is shown in the enlarged view of 2D slice of domain in the Figure 2. Here the distance field and the corresponding medial axis is computed with respect to the geometry and the cylindrical far-field thus avoiding effect of the inlet and exit boundaries. The solid lines represent the shock features i.e. the medial axis and the dashed lines show the expansion features. Following this medial axis branches and even connecting the hanging and expansion features, a poor quality blocking would be achieved. This is also because, to generate the blocks, very small branches of the medial axis between the internal aeroengine geometry parts would have to be combined with very large branches between the aeroengine and the far-field.

To overcome this limitation, the distance field function d can be used. An isosurface (contour in 2D) of d is wrapped around the geometry to facilitate the MAT based block topology generation. The wall distance computation is an intermediate step in the distance field based medial axis approximation and hence is available for use without any extra cost. Thus using an isosurface of the distance field instead of the farfield for the medial axis computation can significantly improve the medial axis based blocking. The hybrid blocking procedure is described below with the help

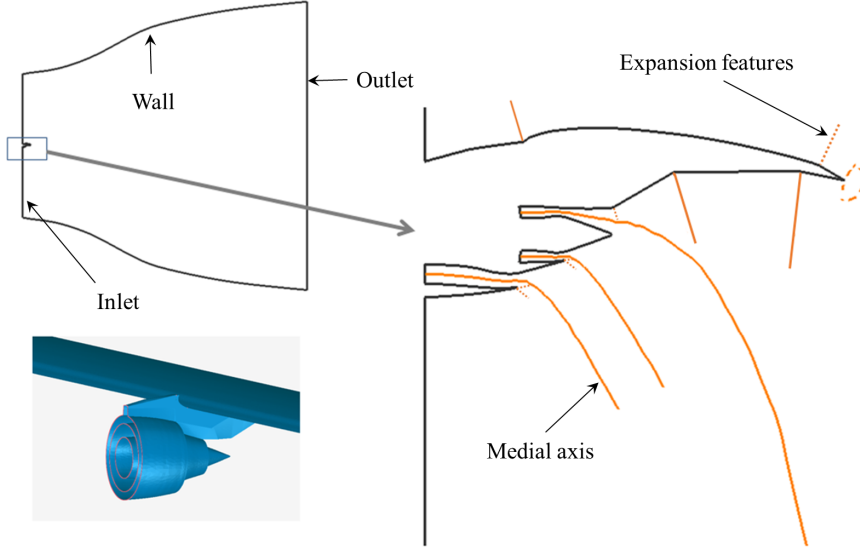


Fig. 2: Jet-wing-flap: medial axis transform (compression shock) and expansion features close to the geometry.

of a simple 2D JWF geomtery. The extension of this methodology to the 3D cases also follows the same procedure as demonstrated later.

- The distance field is computed around the domain of interest as shown in the Figure 3(a). An exact equation for the wall distance d is the hyperbolic eikonal equation which models the front propagation from the surface at unit velocity.

$$|\nabla d| = 1 + \Gamma \nabla^2 d \quad (1)$$

where $\Gamma \rightarrow 0$ yielding viscosity solutions. The first arrival time of the front for a unit velocity is equal to the wall distance. The eikonal equation is solved using a fast marching method [14]. A suitable isosurface is then extracted from d . This isosurface selection is currently arbitrary but it can be linked to a criteria. For example, the width of the shear layer regions in the jet wake can dictate this selection upstream or it could be based upon the dimensionless wall distance y^+ value. The isosurface acts like a virtual geometry or a wrap around the real domain (see 3(b)).

- The next step is approximation of the medial axis between the geometry and the distance field wrap. The Voronoi diagram based algorithm of Dey and Zhao [26] is used here for the medial axis approximation. This algorithm provides a more stable and continuous medial axis for complex 3D domains than the voxel thinning approach. The input to this program is the point cloud data of the geometry and the distance field isosurface. It makes use of the observation that certain Voronoi facets are positioned close to the medial axis if their dual Delaunay edges tilt away from the surface or are very long. Hence, the angle condition and the ratio condition are defined to filter such tilted and long Delaunay edges and the medial axis is approximated.

Let V_P be the Voronoi diagram for a dense point set P from a smooth compact surface $S \subset \mathbb{R}^3$. This Vornoi diagram is a cell complex comprising of Voronoi cells $V_{p \in P}$ and their facets, edges and vertices. Also, for each point $x \in S$,

$$V_p = \{x \in \mathbb{R}^3 \mid \|p - x\| \leq \|q - x\|, \forall q \neq p\} \quad (2)$$

where p and q are any two points in P . Let D_P be the Delaunay triangulation of P and dual to the Voronoi complex. The Delaunay triangles incident to point p which are dual to the Voronoi edges intersected by a tangent plane at p are used to construct the criteria. All the Delaunay edges that make relatively large angle

with the planes of the triangles are filtered. If the angle between the vector \mathbf{t}_{pq} from p to q and the normal \mathbf{n}_{ptu} to a triangle ptu is less than a threshold angle $\frac{\pi}{2} - \theta$ for all the triangles, then that associated Delaunay edge is filtered i.e.

$$\max \angle \mathbf{n}_{ptu}, \mathbf{t}_{pq} < \frac{\pi}{2} - \theta \quad (3)$$

where $0 < \frac{\pi}{2} < \theta$. A value of $\theta = \frac{\pi}{8}$ gives good results. The ratio condition is based on the comparison of the length of the Delaunay edges with the circum-radii of the triangles. Thus those Delaunay edges are filtered which satisfy the criteria:

$$\min \frac{\|p - q\|}{R} > \rho \quad (4)$$

where $\|p - q\|$ defines the length of a Delaunay edge and ρ is the circum-radius of a triangle ptu . A value of $\rho = 8$ is normally used for dense point clouds. The medial axis is generated as a continuous surface which can be imported into the mesh generator. The medial axis for the JWF slice is shown in the Figure 3(c).

- To complete the blocking process, additional rules as described in the Section 1 are manually used. Applying the rules, for example to the 2D JWF slice, the expansion features are connected to the nearest medial vertex or otherwise the medial axis as shown in the Figure 3(d).
- Once the critical parts of the domain have been blocked using the medial axis, the far-field region can be partitioned using simple Cartesian fitting or H-type blocks. This is shown, for example, in Figure 3(d) with the green lines. This resulting domain decomposition is significantly better than the one obtained initially shown in the Figure 2. There can still be some regions where the block topology is unsatisfactory. Such areas must be manually altered. Hence, a semi automatic blocking process arises. The mesh is then generated in the commercial program Pointwise [27].

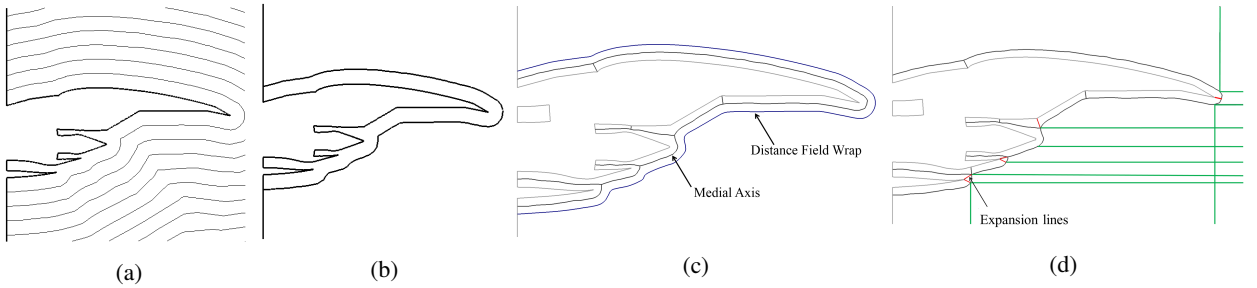


Fig. 3: Two dimensional jet-wing-flap geometry: (a) the distance field; (b) distance field wrap and (c) corresponding medial axis (d) hybrid blocking around 2D geometry.

2.2. Hierarchical geometry handling

Modern day aero-engine design challenges demand performing realistic and multi-scale CFD simulations of strongly coupled systems. This means that geometries are becoming highly complex and as a result more effort is consumed in the mesh generation and flow modeling process. This can have a strong impact on the duration of the design optimization cycle. To this end, a combination of the high and low fidelity (structured multi-block) meshing/modeling techniques can be employed using a hierarchy of the methods shown in the Figure 4. At the bottom of this hierarchy is the smeared representation of the geometry through the use of the lower order methods such as immersed boundary method (IBM) and body force model (BFM) [28,29]. Next in the hierarchy is the real geometry resolved by the over-set meshes which present a useful option for integrating various domains together without adding extra complexity. The information between the overlapping parts is exchanged through interpolation. At the top is the real geometry meshed by, for example, node matching multi-block meshing methods. Therefore, as a cost effective alternative to the fully resolved/meshed geometry, a combination of various high and low fidelity methods allows rapid addition

and modeling of arbitrary geometry effects. This helps in reducing the design cycle time. The objective here is not to present any novel mesh generation method but to apply a zonal/hierarchical approach to handle complex domains to reduce the meshing effort (see Section 3.0.3). Such an approach can be efficiently used to rapidly explore the design space and can aid the development of high fidelity numerical tools.

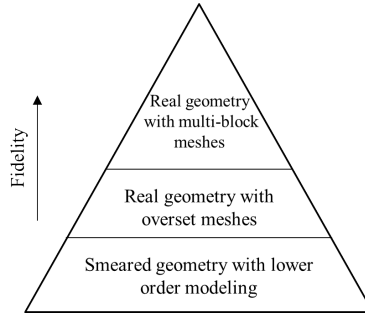


Fig. 4: Hierarchical geometry handling strategy.

2.2.1. Body force modeling

The engine-wing-flap geometry case to be presented later employs the hierarchical geometry handling approach and uses a body force method to model the effect of the fan and outlet guide vanes [30]. This model is outlined next.

Assuming an infinite number of blades, the aerodynamic effects of a blade row are modeled using an axisymmetric flow in each infinitesimal blade passage and the body forces are added as source terms. The parallel and normal components of these forces in cylindrical coordinates system are given as:

$$F_{p,x} = \frac{K_p}{s} V_x V_{rel}, \quad F_{p,\theta} = -\frac{K_p}{s} V_\theta V_{rel}, \quad F_{p,r} = -\frac{K_p}{s} V_r V_{rel} \quad (5)$$

$$F_{n,x} = \frac{K_n}{s} \frac{V_\theta}{V_{rel}} f(V_x, V_\theta, \alpha), \quad F_{n,\theta} = -\frac{K_n}{s} \frac{V_x}{V_{rel}} f(V_x, V_\theta, \alpha) \quad (6)$$

Here, V_x , V_θ and V_r are the axial, tangential and radial velocity components. V_{rel} is the magnitude of the fluid velocity relative to the blade. K_p and K_n are calibration constants. Also, α and s are the local blade metal angle and blade pitch respectively. The above equations can also be modified to produce local blockage terms (see [31]).

3. Results

3.0.1. NASA CRM wing-body-tail

In this section, the hybrid blocking is applied to partition the domain around a 3D NASA Common Research Model (CRM) horizontal wing-body-tail configuration. This model represents a modern, transonic and commercial aircraft designed to cruise at $M = 0.85$ and $C_L = 0.5$. The geometric and aerodynamic details about the model are described in [32,33]. The configuration is shown in the Figure 5(a). The far-field is represented by a cube with boundaries ten fuselage lengths away upstream and downstream and ten spans away from the symmetry plane. First, the distance field wrap is computed around the model geometry which is shown in the Figure 5(b).

The medial axis is approximated around the model wrapped by the distance field isosurface. A cut section of the model geometry and the medial axis is shown in the Figure 5(c). As can be seen, the medial axis branches at the wing-fuselage junction providing a useful block partitioning. The medial axis around the wing and tail also provides a block topology similar to O-type or C-type meshes. To assist the blocking as shown in the Figure 6(a), expansion features at the trailing edges of the wing and the tail are joined to the nearest medial axis. After the blocking around the geometry is complete, the far-field domain partitioning is carried out. The region is partitioned to create a H-type mesh. The block topology around the model is shown in the Figure 6(c). The volume and the surface mesh cuts are

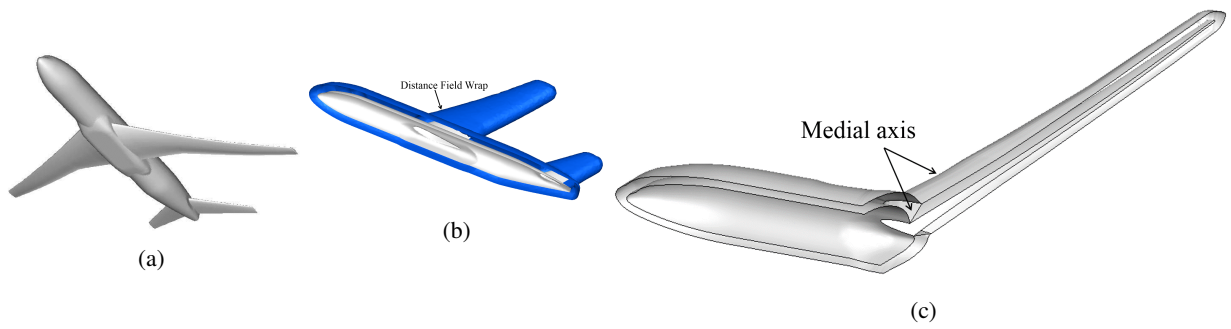


Fig. 5: NASA CRM: (a) wing-body-tail configuration (b) configuration with the distance field wrap (c) cut section with the medial axis.

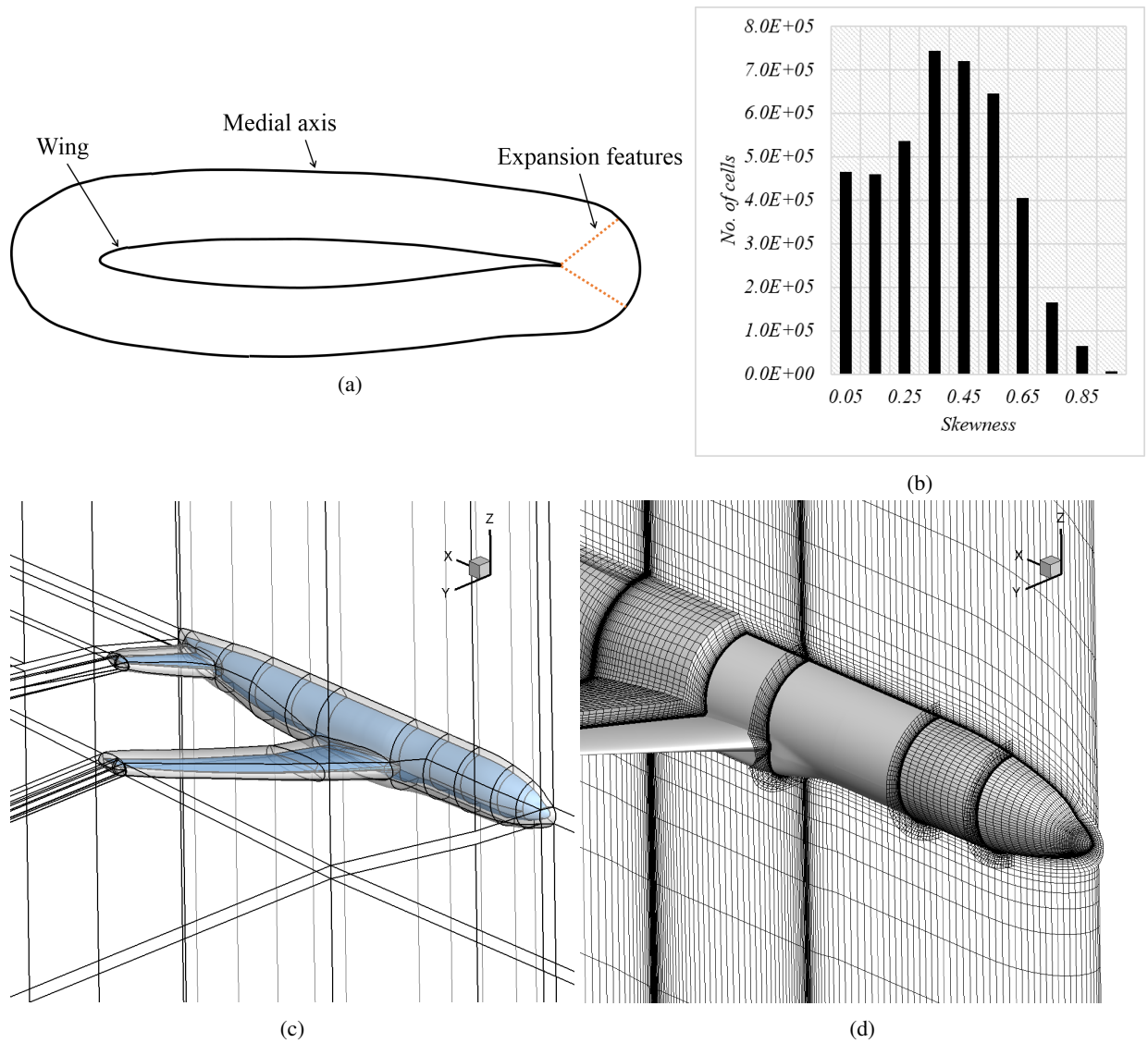


Fig. 6: NASA CRM wing-body-tail (a) blocking around the wing section (b) cell skewness histogram (c) hybrid blocking (d) mesh cut section.

displayed in the Figure 6(d). The cell skewness histogram of the resulting mesh is shown in the Figure 6(b) where approximately 85% of the cells have skewness value below 0.55 (the ideal value being zero).

The NASA CRM configuration has been the test case for the 4th and 5th AIAA CFD drag prediction workshops [33,34]. The aim of the workshop is to assess the state-of-the-art in the CFD methods for aircraft aerodynamic analysis. Here, we use the same flow conditions as given in the workshop to compute the flow around the test case. The simulations are performed in HYDRA which is an unstructured, finite volume, edge-based and compressible flow solver using MUSCL based flux differencing [35,36].

The simulation is carried out at $M_\infty = 0.85$ and $C_L = 0.5$ with Reynolds number of 5×10^6 based on the reference chord length $C_{ref} = 7.00532 \text{ m}$. Table 1 describes the free-stream flow conditions. A coarse mesh of approximately 4 million cells is used. The first grid node from the wall is located at $y^+ \approx 1$. The SpalartAllmaras (SA) turbulence model is used for this simulation. The flow angle for this mesh to gain $C_L = 0.5$ is $\alpha = 2.36^\circ$.

Table 1: NASA CRM free-stream conditions.

M_∞	0.85
P_{total}	201326.91 Pa
T_{total}	310.93 K

The pressure coefficients at locations 13.06%, 28.3% and 50.24% of the wing span is shown in the Figure 7(a-c). The results are compared with the wind tunnel data at these locations. This experimental data is for C_L values of 0.486 and 0.52 as shown in [34]. A good level of agreement with the measurements can be observed in these plots.

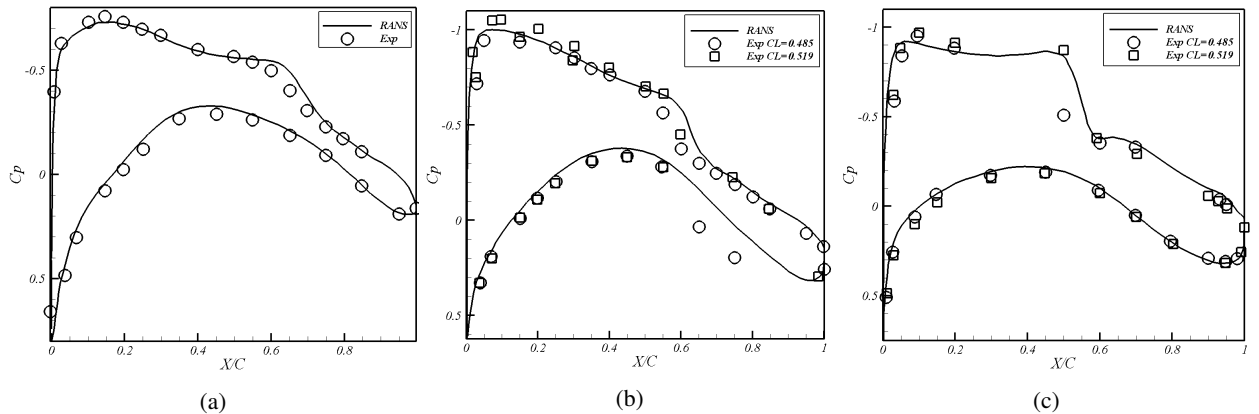


Fig. 7: NASA CRM wing-body-tail (a) pressure coefficients at 13.06% (b) 28.3% and (c) 50.24% of the wing span.

3.0.2. Jet-wing-flap

In this section, the 3D jet-wing-flap case is presented. The geometry comprises of co-axial nozzle, pylon and a wing with a flap as shown in the Figure 8(a). This realistic aero-engine geometry has been used for detailed computational aero-acoustics analysis, as presented, for example in [37,38]. The pylon adds complexity to the otherwise cylindrical nozzle topology along with the wing and the flap. Hence, blocking such a case demands significant user insight. After wrapping the distance field, the medial axis is approximated. This is shown in the Figure 8(b). To simplify the blocking procedure, small medial axis branches are removed for this case. This is followed by the inner blocking aided by the rules which is shown in the Figure 8(c).

The far-field domain decomposition can be then be carried out at this stage. However, one of the aims for the aero-acoustic jet simulations is to properly resolve the shear layers in the far-field. This requires a good quality mesh aligned with the shear layer regions. The current block topology as shown in the Figure 8(c) is non-optimal for properly resolving the shear layers produced by the bypass and the core flows. Hence a manual alteration of the blocking around the pylon and the core flow exhaust is performed. The modified inner block topology with the

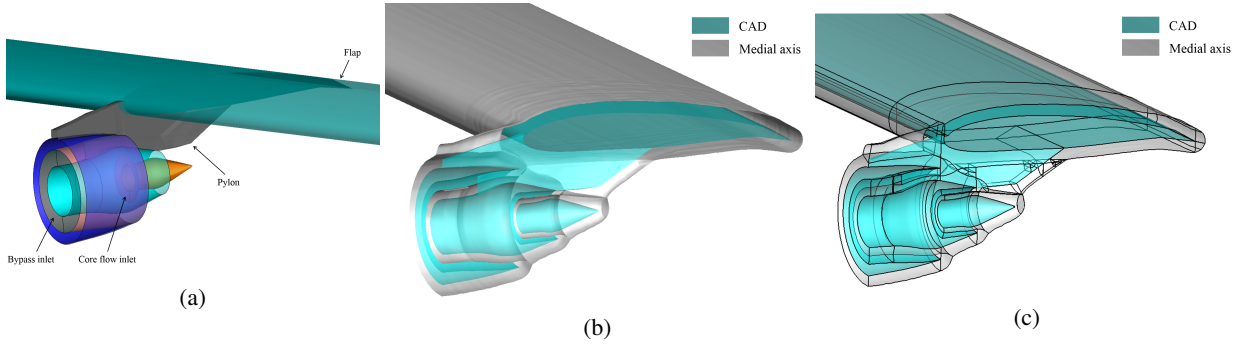


Fig. 8: Jet-wing-flap (a) CAD (b) CAD and the medial axis cut section (c) inner hybrid blocking.

far-field decomposition are shown in the Figure 9(a). Different cut sections of the resulting mesh (20 million cells) showing the surface and volume meshes are displayed in the Figures 9(c) and 9(d).

The cell skewness histogram is shown in the Figure 9(b) demonstrating that the mesh is of good quality. A RANS simulation using the SST $k - \omega$ is carried out on the mesh generated by the hybrid blocking. The first grid node from the wall is located at $y^+ \approx 1$. The jet nozzle boundary conditions for this simulation are given in the Table 2. The mean axial velocity contours at different axial planes are shown in the Figure 10. The results are compared with the experimental data and those obtained from the hybrid RANS-LES simulation performed in [39]. Figure 11 shows an encouraging match where the axial velocity profiles in $z = 0$ plane are plotted. Here, U_o is the bypass exit velocity with value of approximately 300 m/s and D is the bypass jet diameter. The experimental data in these plots is for the clean nozzle jet without the effect of wing and flap, hence a scatter between the CFD and measurements can be seen.

Table 2: Jet nozzle boundary conditions.

	Bypass	Core
P_{total}	171,600 Pa	164,000 Pa
T_{total}	335.0 K	889.0 K
\dot{m}	9.325 Kgs^{-1}	1.633 Kgs^{-1}

The two cases presented above show how the hybrid blocking approach can be effectively used to decompose and mesh the complex geometries. The medial axis based domain decompositions also provide meshes having better flow alignment, as shown in [24,25], when compared to other partitioning methods e.g. Cartesian fitting and cross field based techniques. Hence, this technique further enhances the scope and applicability of these MAT based blocking methods. Also, the blocking templates could be generated using this approach which can speed up the mesh generation process and aid an inexperienced CFD user.

3.0.3. Engine-wing-flap

In the last section, a coaxial nozzle with pylon and wing geometry was presented which makes the rear or downstream part of the aero-engine. To carry out a more realistic simulation, the front engine part containing the axis-symmetric intake, hub and splitter geometry is added to this rear part using the overset mesh at the interface. This procedure avoids re-blocking the domains to have a cell to cell match between the two zones. Also, a smeared fan geometry is used where the fan is modeled using the BFM (see the schematic in Figure 12(a)). The other downstream components are imprinted and treated again with the BFM but with localized sources. These internal geometry components include the downstream vanes, gearbox shaft, and the engine supporting A-frames. Thus using a hierarchical geometry handling approach, a complex domain can be readily meshed and analyzed for in a design optimization cycle.

A cut section of the mesh at $z=0$ plane is shown in the Figure 12(b). The total mesh size is 50 million. The internal geometry in the front part is modeled using a body force model (see section 2.2.1) which has been extended in [40]

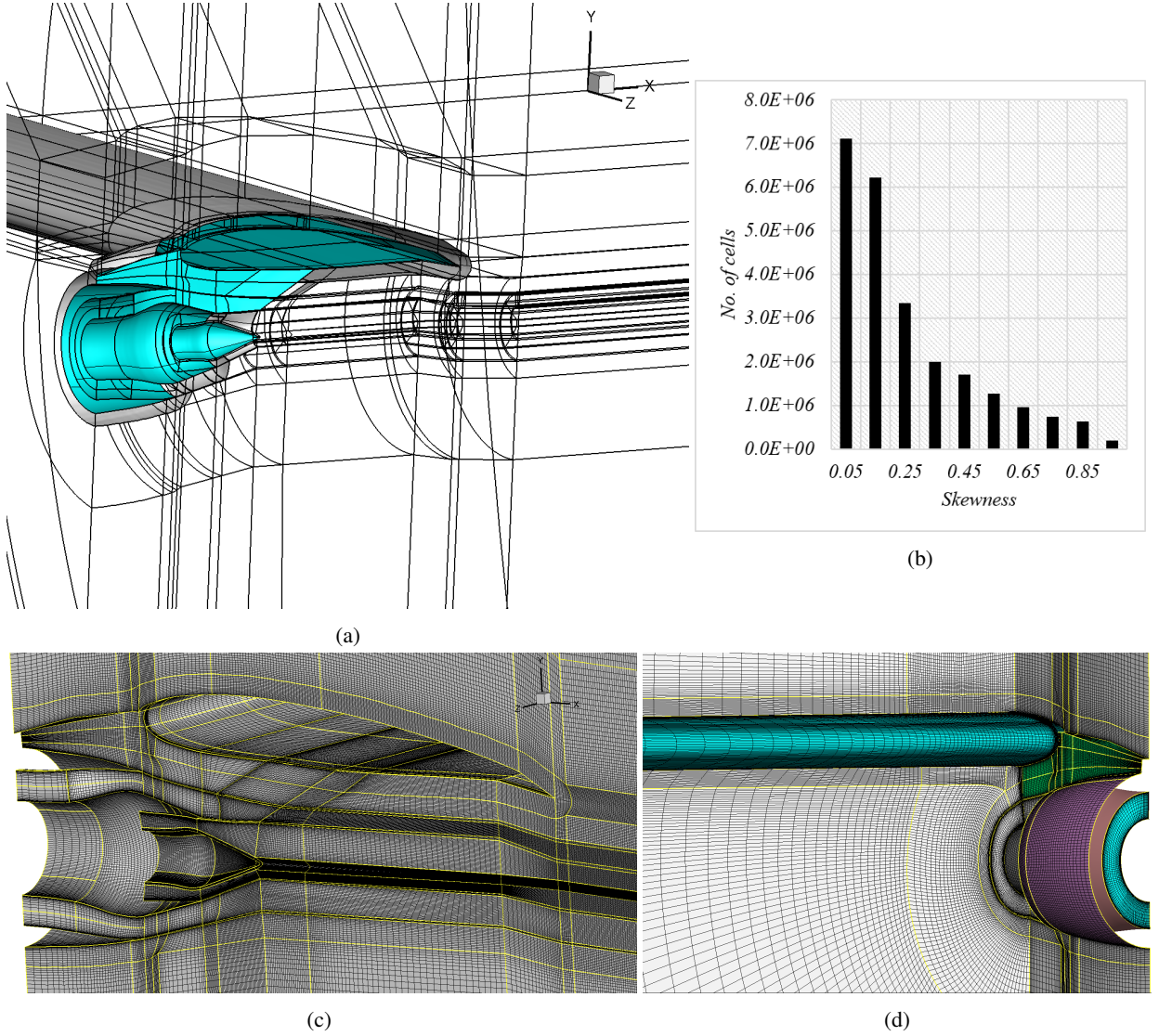


Fig. 9: Jet-wing-flap (a) modified inner blocking (to accommodate shear layers) with far-field block topology surface and volume mesh cut. (b) cell skewness histogram (c) mesh cut section at $z=0$ (d) a surface and volume mesh cut.

to include the local blockage and wakes modeling. This is done by adding local enhanced source terms to generate wake zones, which is similar to adding the source terms in the IBM for simulating geometry or boundary on a non-conformal Cartesian mesh. A unified framework combining smeared geometry and the above mentioned crude IBM has been presented recently in [28,29], which can be an area of future research.

4. Conclusions

In the first part of the paper, a hybrid blocking method is demonstrated that makes use of the distance field isosurface to act as a virtual geometry for the subsequent medial axis computation. Additional rules and the H-type blocking are employed to complete the block topology creation. This extends the original medial axis based method's ability to handle more complex geometries specially the external flows. Practical cases are included to demonstrate the use of this novel method. The short comings of the method for highly complex geometries are also described

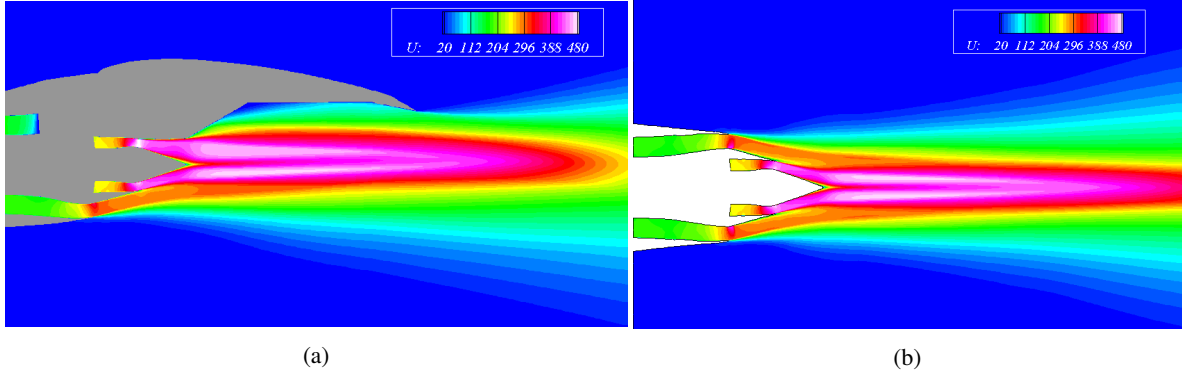


Fig. 10: Jet-wing-flap mean axial velocity contours; (a) $z=0$ plane (b) $y=0$ plane.

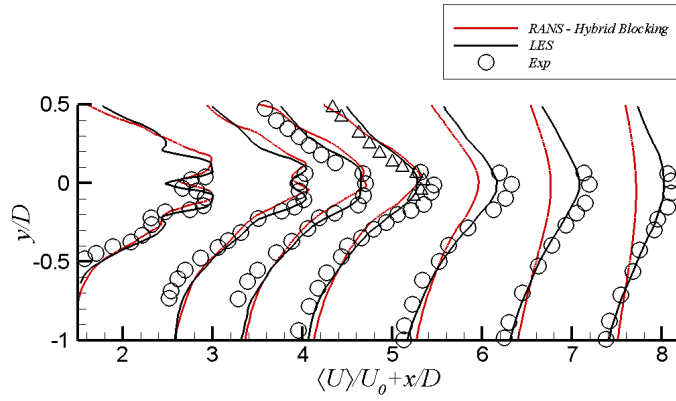


Fig. 11: Jet-wing-flap axial velocity profiles.

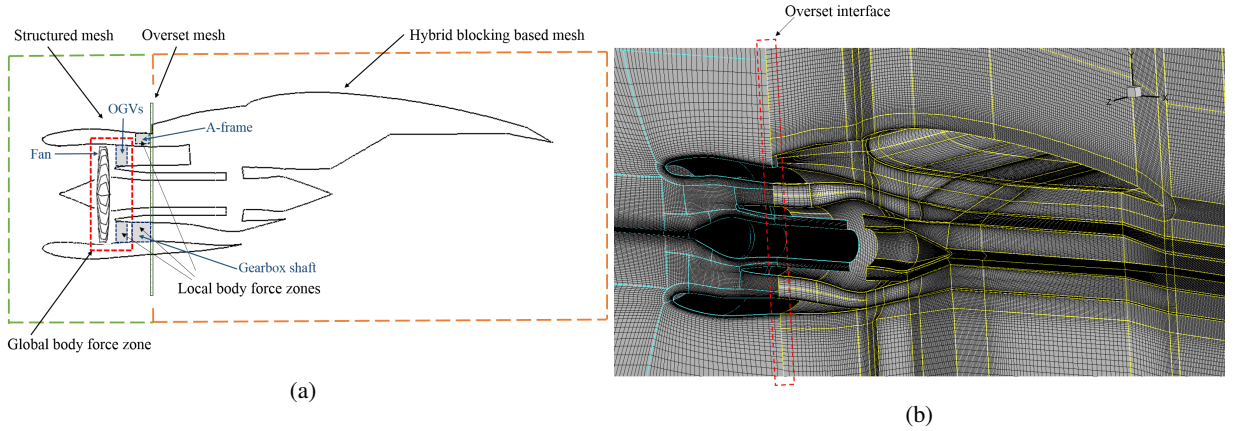


Fig. 12: Engine-wing-flap (a) schematics showing geometric zones and domains with different block topologies (b) cut section at $z=0$ plane.

where manual alteration is required to resolve the important flow features. In the second part of the paper, an alternative to fully resolved and meshed geometry has been presented which handles the geometry by employing lower order modeling, hybrid blocking and the overset meshes. This provides an efficient and cost effective approach for addressing modern day meshing challenges and allows the rapid exploration of the design space.

Acknowledgements

The authors would like to thank the Higher Education Commission, Pakistan and the Rolls-Royce plc for the funding and permission to publish this work. Authors would also like to thank Dr. Caleb Dhanasekaran for providing the technical support and for the useful discussions.

References

- [1] A. Milli, S. Shahpar, PADRAM: Parametric design and rapid meshing system for complex turbomachinery configurations, in: ASME Turbo Expo 2012: Turbine Technical Conference and Exposition, American Society of Mechanical Engineers, 2012, pp. 2135–2148. ASME Paper No. GT 2012-69030.
- [2] T. Tam, C. Armstrong, 2D finite element mesh generation by medial axis subdivision, *Adv. Eng. Software* 13 (1991) 313324.
- [3] M. Price, C. Armstrong, Hexahedral mesh generation by medial surface subdivision: Part I. Solids with Convex Edges, *International Journal for Numerical Methods in Engineering* 38 (1995) 33353359.
- [4] M. Price, C. Armstrong, Hexahedral mesh generation by medial surface subdivision: Part II. Solids with Flat and Concave Edges, *International Journal for Numerical Methods in Engineering* 38 (1995) 33353359.
- [5] D. Sheehy, C. Armstrong, D. Robinson, Computing the medial surface of a solid from a domain Delauney triangulation, in: *ACM Symposium on Solid Modeling Foundations and Applications*, 1995, pp. 201–212.
- [6] T. D. Blacker, R. J. Myers, Seams and wedges in Plastering: A 3D hexahedral mesh generation algorithm, *Engineering with Computers* 2 (1993) 83–93.
- [7] M. L. Staten, S. J. Owen, T. D. Blacker, Unconstrained paving and plastering: A new idea for all hexahedral mesh generation, in: *Proceedings of 14th International Meshing Roundtable*, Sandia National Lab, 2005, p. 399416.
- [8] H. J. Fogg, C. G. Armstrong, T. T. Robinson, Automatic generation of multiblock decompositions of surfaces, *International Journal for Numerical Methods in Engineering* 101 (2015) 965–991.
- [9] N. Kowalski, F. Ledoux, P. Frey, Block-structured hexahedral meshes for CAD Models using 3D frame fields, *Procedia Engineering* 82 (2014) 59–71.
- [10] D. Rigby, : A technique for automatic multi-block topology generation using the medial axis, NASA/CR FEDSM2003-45527 (2004).
- [11] P.-E. Danielsson, Euclidean distance mapping, *Computer Graphics and image processing* 14 (1980) 227–248.
- [12] I. Ragnemalm, The Euclidean distance transform in arbitrary dimensions, *Pattern Recognition Letters* 14 (1993) 883–888.
- [13] J. Vleugels, M. Overmars, Approximating generalized Voronoi diagrams in any dimension (1995). Technical report UU-CS-1995-14 Utrecht University.
- [14] H. Xia, P. Tucker, Finite volume distance field and its application to medial axis transforms, *International Journal for Numerical Methods in Engineering* 82(1) (2010) 114134.
- [15] H. Xia, P. Tucker, Fast equal and biased distance fields for medial axis transform with meshing in mind, *Applied Mathematical Modelling* 35 (2011) 580419.
- [16] P. Tucker, Differential equation-based wall distance computation for DES and RANS, *Journal of Computational Physics* 190(1) (2003) 229248.
- [17] D. Bommes, T. Lempfer, L. Kobbelt, Global structure optimization of quadrilateral meshes, in: *Computer Graphics Forum*, volume 30, Wiley Online Library, 2011, pp. 375–384.
- [18] Y. L. i, W. Wang, R. Ling, C. Tu, Shape optimization of quad mesh elements, *Computers & Graphics* 35 (2011) 444–451.
- [19] J. Palacios, E. Zhang, Rotational symmetry field design on surfaces, in: *ACM Transactions on Graphics (TOG)*, volume 26, ACM, 2007, p. 55.
- [20] N. Kowalski, F. Ledoux, P. Frey, A PDE based approach to multidomain partitioning and quadrilateral meshing, in: *Proceedings of the 21st international meshing roundtable*, Springer, 2013, pp. 137–154.
- [21] H. J. Fogg, C. G. Armstrong, T. T. Robinson, Enhanced medial-axis-based block-structured meshing in 2-D, *Computer-Aided Design* (2015).
- [22] W. R. Quadros, LayTracks3D: a new approach to meshing general solids using medial axis transform, *Procedia Engineering* 82 (2014) 72–87.
- [23] I. Malcev, Automated blocking for structured CFD gridding with an application to turbomachinery secondary flows, in: *20th AIAA Computational Fluid Dynamics Conference*, Honolulu, Hawaii, 2011.
- [24] Z. Ali, P. G. Tucker, Multiblock structured mesh generation for turbomachinery flows, in: *Proceedings of the 22nd International Meshing Roundtable*, Springer, 2014, pp. 165–182.
- [25] Z. Ali, Optimal block topology generation for CFD meshing, Ph.D. thesis, Department of Engineering, University of Cambridge, UK, 2015.
- [26] T. K. Dey, W. Zhao, Approximate medial axis as a Voronoi subcomplex, *Computer-Aided Design* 36 (2004) 195–202.
- [27] Pointwise, <http://www.pointwise.com>.
- [28] T. Cao, P. Hield, P. G. Tucker, Hierarchical immersed boundary method with smeared geometry, in: *54th AIAA Aerospace Sciences Meeting, AIAA Science and Technology Forum and Exposition*, 2016, pp. 2016–2130.
- [29] T. Cao, N. R. Vadamani, P. G. Tucker, A. R. Smith, M. Slaby, C. T. J. Sheaf, Fan-intake interaction under high incidence, in: *Proc. of ASME Turbo Expo*, Seoul, South Korea, 2016. ASME Paper Number GT2016–56561.
- [30] Y. Gong, A computational model for rotating stall and inlet distortions in multistage compressors, Ph.D. thesis, PhD thesis, Massachusetts Institute of Technology, Cambridge, USA, 1999.
- [31] P. G. Tucker, *Unsteady Computational Fluid Dynamics in Aeronautics*, Springer, 2013.
- [32] J. C. Vassberg, M. A. DeHaan, S. M. Rivers, R. A. Wahls, Development of a common research model for applied CFD validation studies (2008). AIAA Paper No. AIAA-2008-6919.

- [33] J. Vassberg, E. N. Tinoco, M. Mani, B. Rider, T. Zickuhr, D. Levy, O. P. Brodersen, B. Eisfeld, S. Crippa, R. A. Wahls, et al., Summary of the Fourth AIAA CFD Drag Prediction Workshop (2010). AIAA Paper No. AIAA-2010-4547.
- [34] D. W. Levy, K. R. Laflin, E. N. Tinoco, J. C. Vassberg, M. Mani, B. Rider, C. Rumsey, R. Wahls, J. H. Morrison, O. P. Brodersen, et al., Summary of data from the fifth AIAA CFD drag prediction workshop (2013). AIAA Paper No. AIAA-2013-0046.
- [35] L. Lapworth, Hydra-CFD: a framework for collaborative CFD development, in: International Conference on Scientific and Engineering Computation (IC-SEC), Singapore, June, volume 30, 2004.
- [36] P. Moinier, Algorithm developments for an unstructured viscous flow solver, Ph.D. thesis, Oxford University, 1999.
- [37] H. Xia, P. G. Tucker, S. Eastwood, M. Mahak, The influence of geometry on jet plume development, *Progress in Aerospace Sciences* 52 (2012) 56–66.
- [38] J. Tyacke, M. Mahak, P. G. Tucker, LES of jet flow and noise with internal and external geometry features, AIAA Paper No. AIAA-2015-0503 (2015).
- [39] S. Eastwood, P. G. Tucker, Hybrid LES-RANS of complex geometry jets, *International Journal of Aeroacoustics* 10 (2011) 659–684.
- [40] S. Loiodice, P. G. Tucker, J. Watson, Modeling of coupled open rotor engine intakes, in: Proceedings of the 48th AIAA Aerospace Sciences Meeting and Exhibit, Orlando, FL, January, 2010, pp. 4–7. AIAA Paper No. AIAA-2010-840.